JOURNAL OF MATERIALS SCIENCE 18 (1983) 2029–2046

Fracture behaviour of collimated thermoplastic poly(ethylene terephthalate) reinforced with short E-glass fibre*

C. LHYMN, J. M. SCHULTZ
Center for Composite Materials, University of Delaware, Newark, DE 19711 USA

The fracture behaviour of thermoplastic poly(ethylene terephthalate) reinforced with short E-glass fibre was investigated using fractography and a fracture mechanics approach. The observed microstructures, crack propagation and the stress–rupture lifetime data indicate a sudden breakdown induced by far-field effects. The critical damage appears to be correlated with a ductile-to-brittle transition of matrix fracture. The calculation of fracture toughness for various fibre orientations indicates that the fibre pull-out energy is the dominant term in the case in which the fibre orientation is perpendicular to the notch tip.

1. Introduction

Composite injection-moulding compounds consist of short fibres dispersed in a thermoplastic matrix. Injection-moulding compounds have an advantage over short-fibre sheet-moulding compounds (thermosetting matrix) and continuous fibre systems because of the possibility of moulding complex shapes. The principal disadvantages are the relatively soft matrix and a present lack of predictability of the ultimate properties. Of primary concern in the ultimate mechanical behaviour is the orientation distribution of and interactions among the fibres.

All previous work on injection-moulding compounds has utilized as-moulded material. Such material is extremely inhomogeneous, exhibiting surface layers in which fibres are oriented in the mould-fill direction (MFD) and a core in which the fibres are preferentially aligned normal to the MFD [1–4]. In such a circumstance, it is difficult to study the mechanisms of failure because of the added complications of the orientation inhomogeneity. In the present study, single-ply material has been used and failure behaviour has been followed.

Both fractography and linear elastic fracture mechanics (LEFM) have been used to characterize failure. With regard to the use of LEFM, this approach has been found of general utility in composite fracture work [5–13], and its utility in characterizing failure in short-fibre composites has recently been demonstrated [1–3, 14].

A recent study of polyamide thermoplastic reinforced with short glass and graphite fibres [15] demonstrated that the failure is likely to initiate at fibre ends. The proposed damage model [16] implies specimen breakdown in a critical cross-section that has been weakened by the accumulation of cracks. The above model of a bridging zone was approached using probability theory, assuming that the failure of the composite occurs due to the inability of the short fibres bridging a critical zone to carry the load [17].

The present work will reveal the structural model of sudden breakdown based on a far-field effect. Also, the concept of a critical crack length will be introduced to explain the ductile-to-brittle transition in the fracture mode with respect to a sudden catastrophic failure.

2. Experimental details

Rynite® 545, an injection moulding compound, consisting of a thermoplastic poly(ethylene terephthalate) (PET) matrix filled with approxi-

*Work supported by the University–Industry Research Program, Center for Composite Materials.

0022–2461/83 $03.00 + .12

mately 45 wt% chopped E-glass fibres, was used throughout this work. The diameter of the fibre is 12 μm. The material was injection moulded into 5″ x 7″ x 1/8″ (12.7 cm x 17.8 cm x 0.32 cm) plaques, using an end-gated mould. It has recently been shown, for this material, that the fibre orientation varies systematically across the specimen thickness [1–3]. Near the mould surface, the fibres are aligned in the mould-fill direction (MFD); in the centre section, distant from the surface, the fibres are oriented in the plane of the plaque and approximately normal to the MFD.

A fracture plane containing the thickness direction and the normal to the MFD is shown in Fig. 1. The two surface layers and the orthogonally oriented core are easily seen. To obtain a single layer ply, the as-moulded three-layer laminate is machined from one side only to 1/3 of the initial thickness. This process effectively eliminates one outer layer and the "core".

Compact tension specimens are used in this work. The specimen dimensions are shown in Fig. 2. These dimensions are smaller than those specified by ASTM E399-74. Two reasons why the reduced size is chosen are:

1. Elimination of instability-related shear fracture mode. This problem plagued the early phases of this work, but was finally obviated by the relatively short geometry of Fig. 2, and also by the use of lateral constraints.
2. Reduction of specimen warpage.

Three kinds of machine-notch geometry are used: L-specimen ($\theta = 90°$), 45°-specimen ($\theta = 45°$), and T-specimen ($\theta = 0°$). Here, θ denotes the angle between MFD and notch.

For thin specimens (0.10 cm on average), it was found impossible to maintain the planar shape of the sample when the load is high (instability). The phenomenon of instability is illustrated in Fig. 3. When such instability develops, the crack propagation and final fracture mode become shear-like. Such an instability was eliminated by decreasing the notch-crack distance, a, so that mode I fracture was accomplished instead of mode III in the case of L-specimens. Specifically modified metal side support plates [18] were employed also to inhibit mode III shear fracture. But it was discovered that this metal fixture could not prevent shear fracture always, because, when the shear stress becomes extremely high, the metal fixture itself could not maintain the planar shape. It is only effective under a low shear stress acting on the sample.

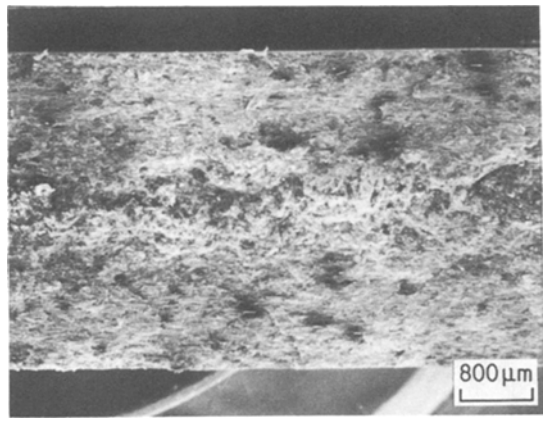

Figure 1 Fibre distribution along the thickness (1/8 inch) direction (↕). The MFD is perpendicular to the plane of the paper. This is a natural three-layer laminate caused by the process of injection moulding.

The as-injection moulded, rectangular plaque warps during the machining to about 1/24 inch thickness, probably due to internal stresses. Typical warpage is 5 mm over a 12.5 cm length.

Tensile specimens used for constant strain rate tensile testing are of dog-bone geometry, with a 9.53 mm gauge length, radii of 12.7 mm radius and a 3.18 mm x 3.18 mm cross-section.

Static stress-rupture experiments are economically instrumented as illustrated in Fig. 4. Here a specimen failure trips a switch (s_n) from the normal a_n connection to b_n connection, which changes the input voltage to a strip chart recorder. The pen motion on the recorder indicates both which specimen has failed and when. The switch is normally connected to position a_n ($n = 1, 2, \ldots, n$) but, when the specimen is fractured completely, is connected to position b_n by the mechanical process shown in Fig. 10b. Different values of R_n cause a different step height in a time-based chart recording signal.

3. Results

3.1. Crack propagation

3.1.1. Crack propagation of L-specimens under static loading

The typical behaviour for crack propagation under an air environment is as follows. Under an initially applied load, the crack grows to a certain length and then further growth is virtually stopped (crack arrest). When the load is increased a little, the crack propagates suddenly to fracture after a certain duration of holding time. The stage of classical crack acceleration [19] was impossible to

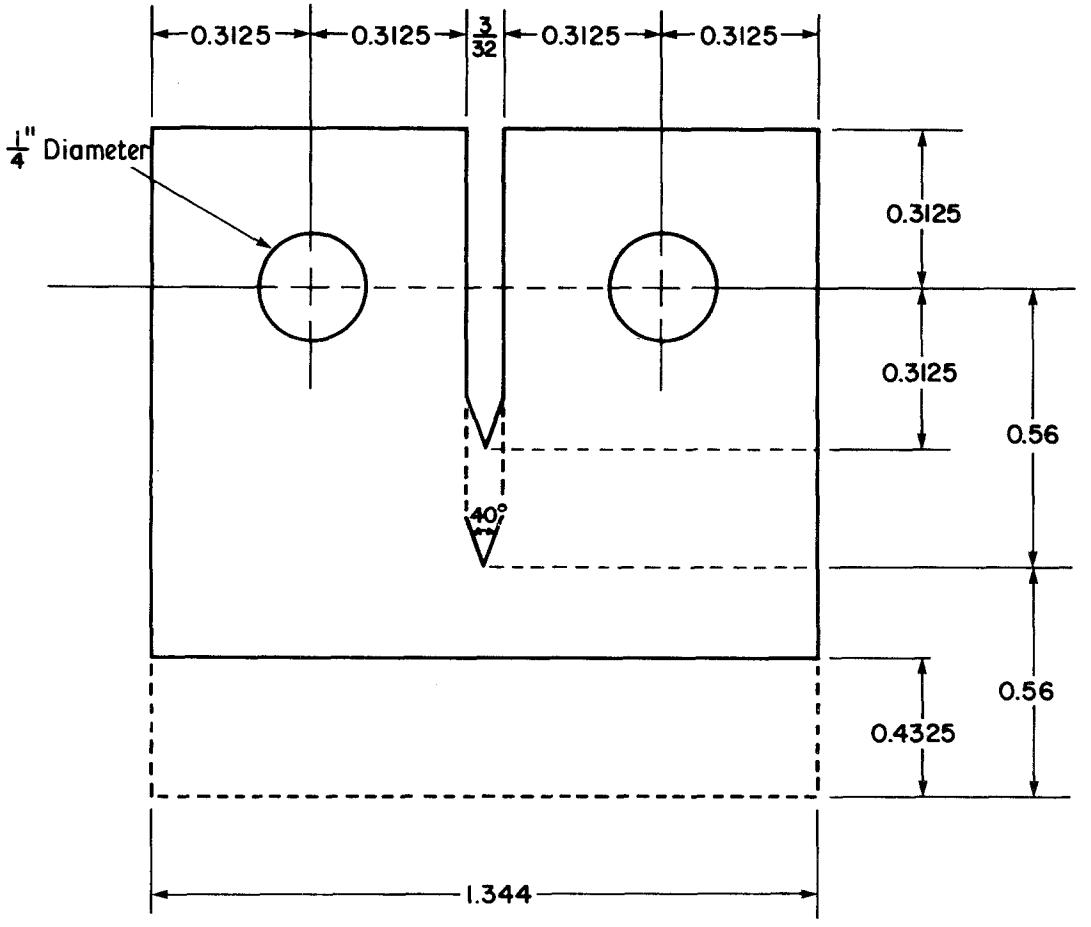

Figure 2 Geometry of compact tension specimen. (Extended dotted line size is the reduced version of ASTM designation: E399-74.)

detect, due to the instantaneous failure. The initial stage of crack growth is discontinuous, the crack propagating in a step-wise fashion, as illustrated in Fig. 5.

Crack propagation has been followed by microscopic examination of the surfaces of the compact tensile specimens. Fig. 6 shows optical micrographs of the early stages of crack propagation. Fig. 7 is a scanning electron micrograph from the vicinity of the tip of a growing crack. As can be seen, scanning electron microscopy is especially sensitive to small fractures, since those fissures are not accessible to the evaporated gold coating and consequently act as sites of electrostatic charging.

These micrographs are typical of what is observed. A summary of the observation is:

1. The crack path has an irregular, zig-zag shape, but propagates along the centre line, on average.
2. Microcracks develop at the fibre ends. The voiding of a fibre end is shown at larger magnification in Fig. 8. The detachment of the matrix at the interface results in the formation of microcracks, which finally coalesce to form a continuous crack under the necking and yielding of the crazed matrix between them. The coalescence has formed a continuous yielded zone, which is torn apart, leaving individual dimples of stretched matrix material.
3. Interfacial debonding follows the fibre-end microcracking.
4. A large degree of fibre fracture is observed. This fibre fracture is induced by the combined action of tensile stress and shear stress. The shear stress from the neighbouring fibre tip is transferred through the matrix. There appears to be a critical distance, above which the shear stress is not effective in inducing a

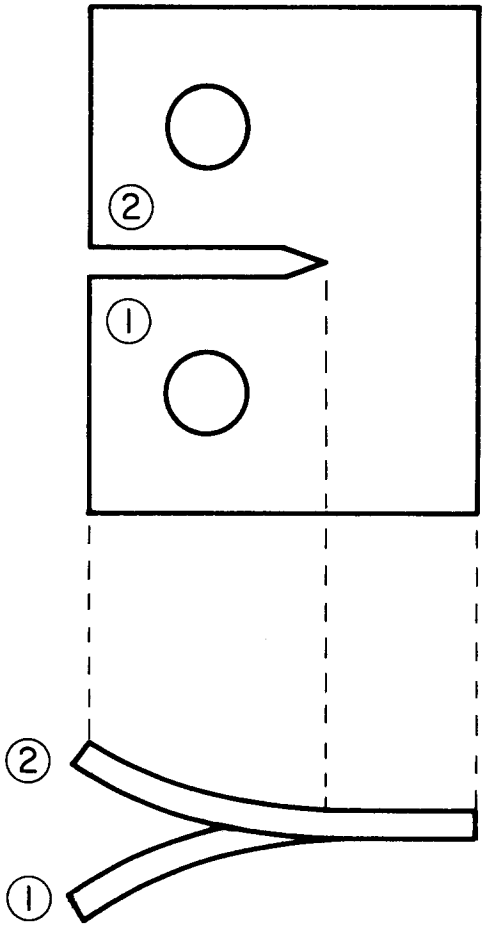

Figure 3 The mode of instability. When the load becomes high, the thin sheet specimen (0.10 cm thick) takes the position indicated in the top view.

fibre fracture. The net result of the interaction of a neighbouring fibre end is the increased tensile force on the surface of the adjacent fibre.

5. Generally, the fibre fracture is accomplished long before the general crack tip arrives. When the crack tip meets a fibre which is not fractured previously, interface debonding and fibre pull-out is the mechanism of crack propagation.

3.1.2. Crack propagation of T-specimens under static loading

Crack propagation data for two T-specimens are shown in Fig. 9. There is a step-wise crack growth; however, this behaviour is diminished with respect to L-oriented specimens.

A typical crack tip micrograph is shown in Fig. 10. The fracture mechanism is mainly interface debonding plus matrix cracking, a critical process being the matrix crazing to join microcracks. That is, the interface failure is seen far ahead of the front of the continuous crack; joining-up is the only remaining obstacle. Fibre fracture is still visible, but its role is minor.

Matrix cracking is believed to be preceded by crazing. (Molecules become oriented in fibrils at a small angle to the stress axis.) Individual crazes increase in density with increasing load time until they coalesce to form a continuous band of yielding and necking. This zone later tears apart, at first at individual holes, to form a continuously cracked plane.

3.1.3. Crack propagation of 45° – specimens under static loading

Crack propagation data for a specimen with fibres at 45° to the tensile axis is shown in Fig. 11. Again, the crack propagation is discontinuous, but much less so than for L-specimens.

Fig. 12 is typical of the crack morphology seen in this orientation. The following points can be drawn:

1. The crack grows along the fibre axis.
2. Several cracks grow concurrently and the topological connection of such branches is the growth process of the main crack tip.
3. A matrix crack grows by a crazing process, as shown in Fig. 13.
4. The role of fibre fracture is less significant than it is for the L-geometry.

3.1.4. Fatigue crack propagation

Crack propagation data for L- and T-specimens are given in Figs. 14 and 15. The shape of the crack propagation curve for 45° material is similar. Two features are evident:

1. The crack velocity is quite constant; i.e. a quasi-linear behaviour of a N relationship is observed. Plotting da/dN against ΔK_I, the curve fluctuates about a constant level.
2. Discontinuous crack growth is again seen.

A series of micrographs were taken during interruption of a tension–tension sinusoidal load-control fatigue experiment (5 Hz, maximum load = 10 kg, $R = 0.22$) of a L-specimen. Excerpts from that series are given in [18]. It is clear that the crack propagates by interface debonding and ultimate pull-out, plus matrix cracking. Fibre fracture is observed only in the far field, never near the main crack tip. Again, the connecting of

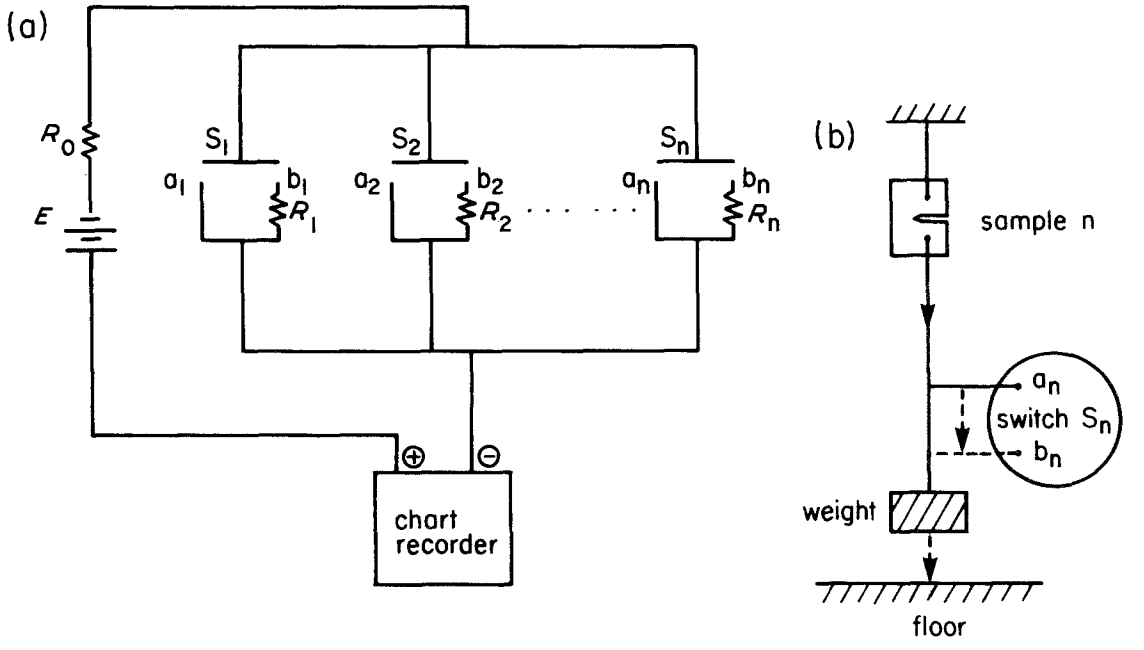

Figure 4 Instrumentation for economical stress-rupture test of many specimens. (a) Electronics. (b) Mechanical: dotted line is the case of specimen breakdown.

far-field microcracks is critical to the failure process.

A recent study on fatigue crack propagation in graphite fibre-reinforced (discontinuous fibre) Nylon 66 [20] reports a constant flaw propagation rate for almost the whole life except only in the last few cycles of crack acceleration. The mechanism proposed was that the damaged zone around the flaw tip grows linearly with time until the material has been weakened enough to cause rapid failure. The present study indicates the same linear growth behaviour, but the connectedness of several discrete microcracks is a new consideration.

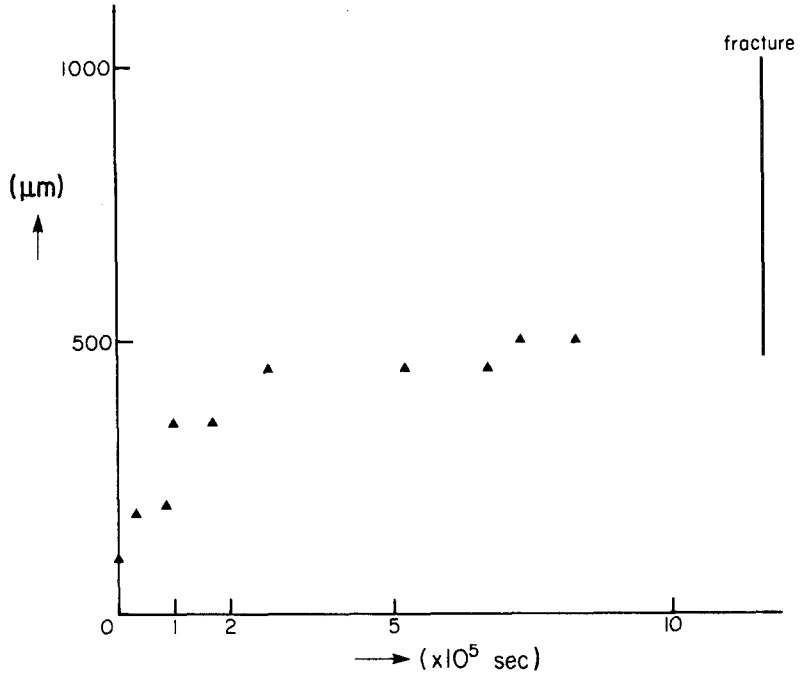

Figure 5 Static crack growth of L-specimen under a constant load (12.9 kg).

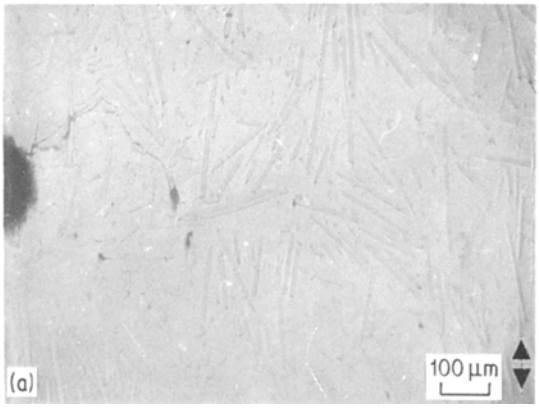

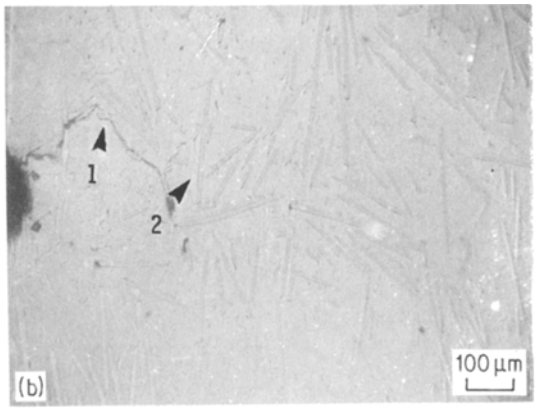

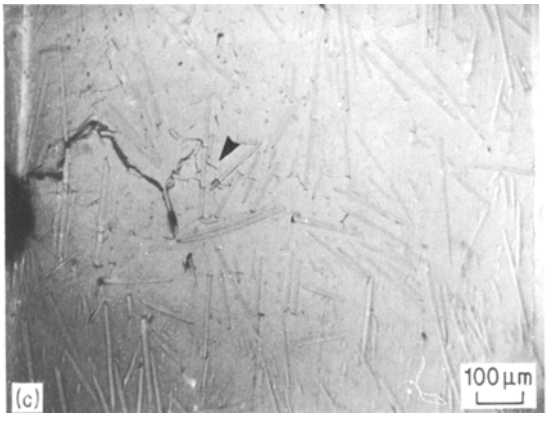

Figure 6 Optical micrographs showing early stages in the propagation of a crack in a L-oriented compact tensile specimen. (a) Constant load: 9.08 kg). The black arc at the far left centre is the tip of a machined-notch crack. Generally, the crack propagates through the matrix and the matrix/fibre interface. (b) Same as (a), but later. First arrow indicates interfacial debonding and second arrow indicates fibre fracture. (c) Constant load increased to 9.67 kg. The arrow indicates matrix cracking.

3.2. Matrix fracture morphology

The examination of fracture surfaces is useful in providing information regarding mechanisms of failure. As was pointed out above, fibre fracture or debonding can occur well ahead of the general crack. Connectivity of such far-field microcracks, though matrix deformation and failure, is necessary to crack propagation. The fracture surface contains information on the failure history of the matrix and is examined here in that context.

3.2.1. Stress-rupture

The stress-rupture test is a constant loading situation and there is no limit on strain rate. Initially, the stress is concentrated near the notch tip and a crack grows slowly. But as the crack length increases, the stress concentration factor increases and then finally crack instability

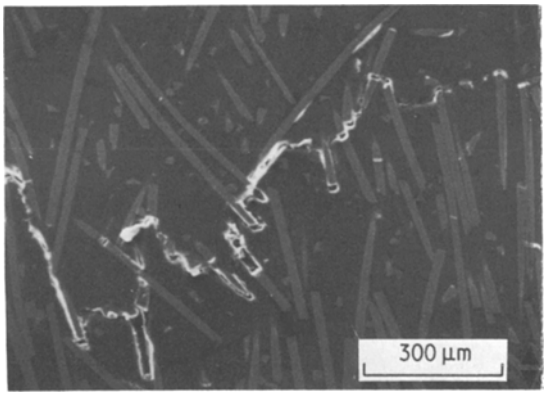

Figure 7 SEM view along a crack path.

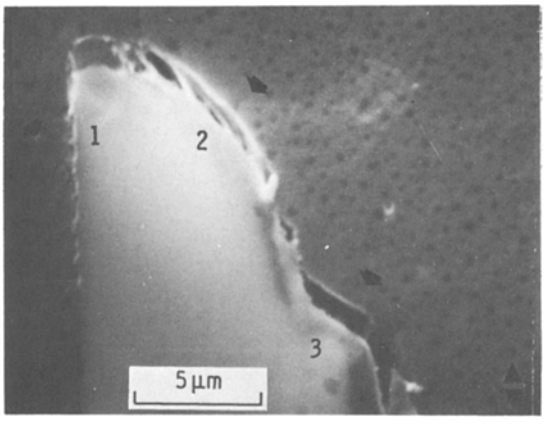

Figure 8 Voiding, crazing and microcracking at fibre end. First arrow indicates void formation under shear stress; second arrow indicates crazed matrix; third arrow indicates detached matrix-induced microcracks. (18.25 kg vertical loading.)

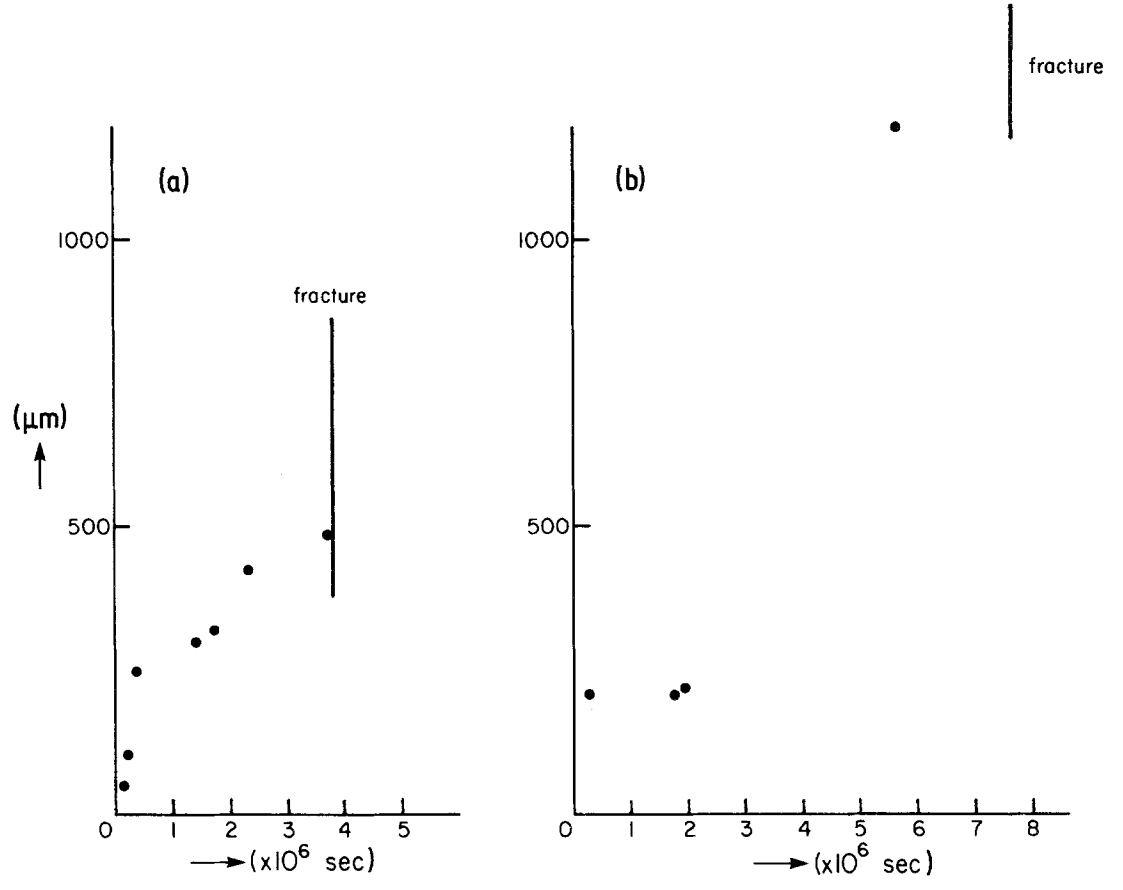

Figure 9 Static crack propagation of T-specimens (a) and (b).

induces a fast (instantaneous) crack propagation. As we have seen, the three-dimensional fracture surface of a L-specimen shows a zig-zag shape, while that of a T-specimen shows a flat fracture surface.

Examination of the matrix for the L-orientation shows a ductile-to-brittle transition along the fracture surface. An example is shown in Fig. 16. Here the matrix near the machine notch shows ductile fracture; the material toward the opposite end

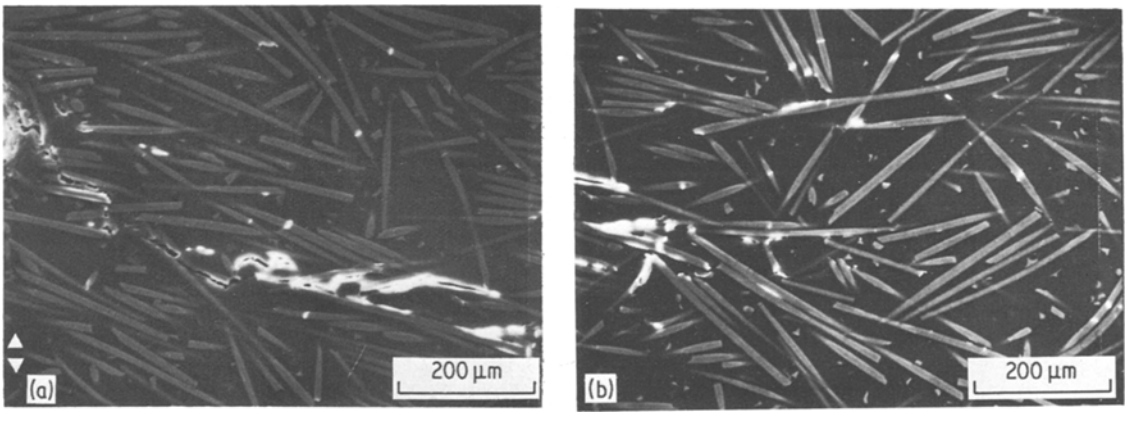

Figure 10 (a) Crack propagation from the notch tip (far left arc) is mainly along the interface in the case of the T-specimen. Matrix crazing is the joining mechanism of pre-existing interface cracks. (b) Crack tip area of (a). Fibre fracture and interface debonding are accomplished far away from the main crack tip (10 kg loading).

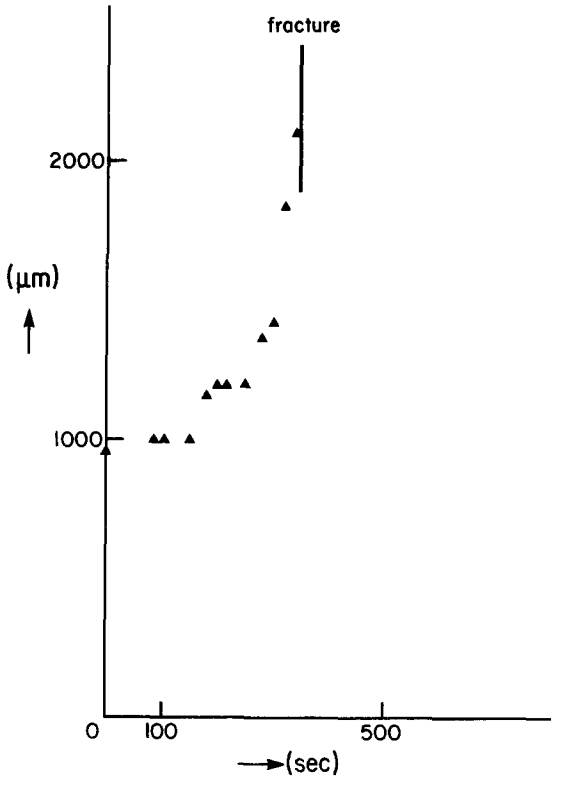

Figure 11 Static crack propagation of 45°-specimen under 7.45 kg load.

shows brittle fracture. The transition occurs at about 3000 μm (values for the three L-specimens measured were 3700, 2800, and 2800 μm).

The following observations derive from the fracture surface micrography:

1. There is a ductile-to-brittle transition from the notch tip to the specimen end.
2. Microcracks initiate from fibre ends by a crazing process (Fig. 17).
3. The shear rupture is produced either from the fibre pull-out process in a ductile zone or from the macroscopic change (not shown) of crack path along the zig-zag pattern in a brittle zone.
4. The ductile-to-brittle transition coincides broadly with slow to fast crack propagation.

The stress-rupture of a typical T-specimen is revealed in the micrographs of Fig. 18. A ductile-to-brittle transition is also seen and the fibre debonding (and also the occasional fibre pull-out by the non-ideal situation of fibre orientation) is generally cohesive. Here, "cohesive" debonding is taken to mean that the residual matrix phase adheres to the fibre surface. The word "adhesive" means that there is no residual matrix phase on the fibre surface. The fracture surface is mainly through the matrix phase, partially through the interfacially debonded or pulled-out fibres. This corresponds with the two-dimensional, external surface crack propagation studies described above.

3.2.2. Constant strain deformation and fatigue

Impact behaviour was mimicked by rapid constant strain rate tensile loading, leading to rupture in less than one second. Fig. 19 is representative of fracture surface observations on such quasi-impact tests. Long lengths of fibre are pulled out of the matrix. In this case, the fibre debonded and the matrix has flowed plastically as the fibres pulled out of their sockets.

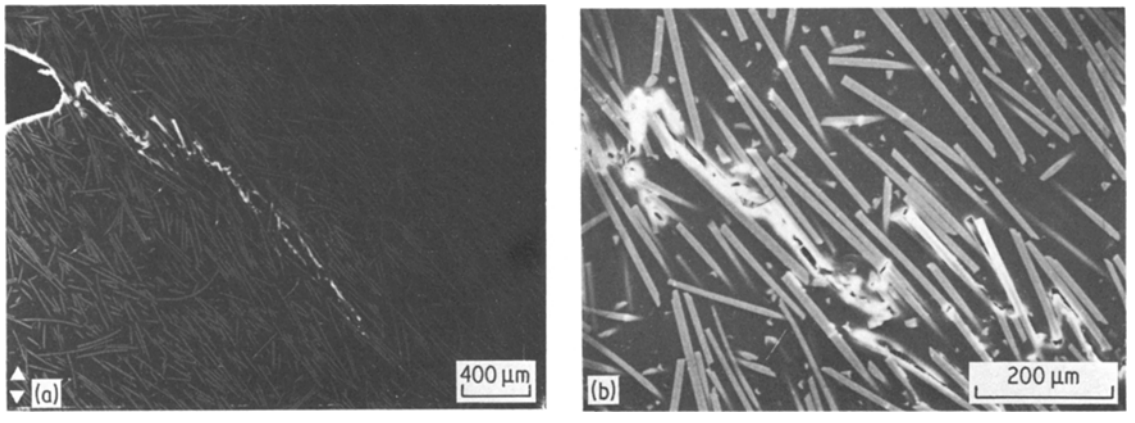

Figure 12 (a) Static crack growth in 45°-specimen. Crack follows the fibre orientation. Several crack branches propagate simultaneously. The connectivity of such branches is the criterion of ultimate failure (10 kg loading). (b) Same as (a) but magnified. Interface debonding is believed to develop through shear stress-induced voiding, cracking and crazing. Fibre fractures are visible away from the crack tip (far-field effect).

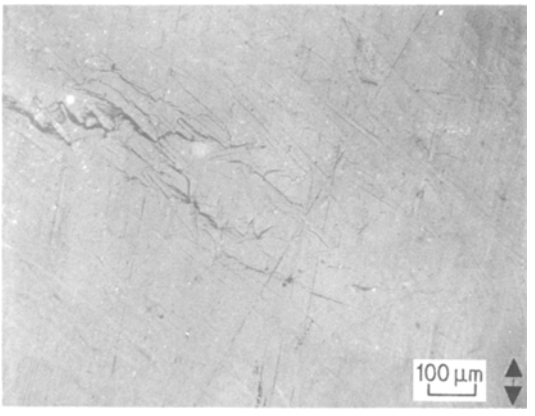

Figure 13 Optical micrograph of 45°-specimen. Enhanced matrix crazing at localized places is one evidence of a far-field effect (7.45 kg loading).

The behaviour in constant load amplitude fatigue is considerably different. For both L- and T-orientation, the initial matrix failure is planar and apparently brittle. At a later stage, the matrix fails ductilely. Equally significantly, there are no long lengths of fibre pulled out, but rather the fibre activity is characterized by massive fracture and short pull-out lengths. An example from the transition region between brittle and ductile zones is shown as Fig. 20.

It is likely that the fatigue is strongly related to the quasi-impact behaviour. A plausible scenario is that debonding and some fibre pullout occur near the crack tip during the tension stroke. On the reverse stroke the fibre can buckle and fracture brittlely. The absence of extensive fibre pull-out and the massive fibre fracture are thereby explained. Possibly the initial apparently brittle failure of the matrix is related to the planar shape of the fibre fracture; when a fibre fractures near the crack tip, the stress is locally raised and the failure proceeds along the plane of the fibre fracture. This should occur as long as the mean stress is not high enough to produce microcracking in the far field. When far-field microcracking occurs, the crack is led out of its plane, in order to join the microcracks. Matrix deformation and flow become an important part of this latter behaviour.

3.3. Stress-rupture lifetime

The stress intensity-factor equation for compact tension specimens can be presented in the form [21]:

$$K_c = \frac{P}{B/a^{1/2}} f\left(\frac{a}{w}\right) \quad (1)$$

where P is the applied load, B is the specimen thickness, and $f(a/w)$ is a measure of the compliance of the specimen. K_c is defined as the value of the stress intensity factor K_I at which a crack in the specimen begins to grow before being arrested.

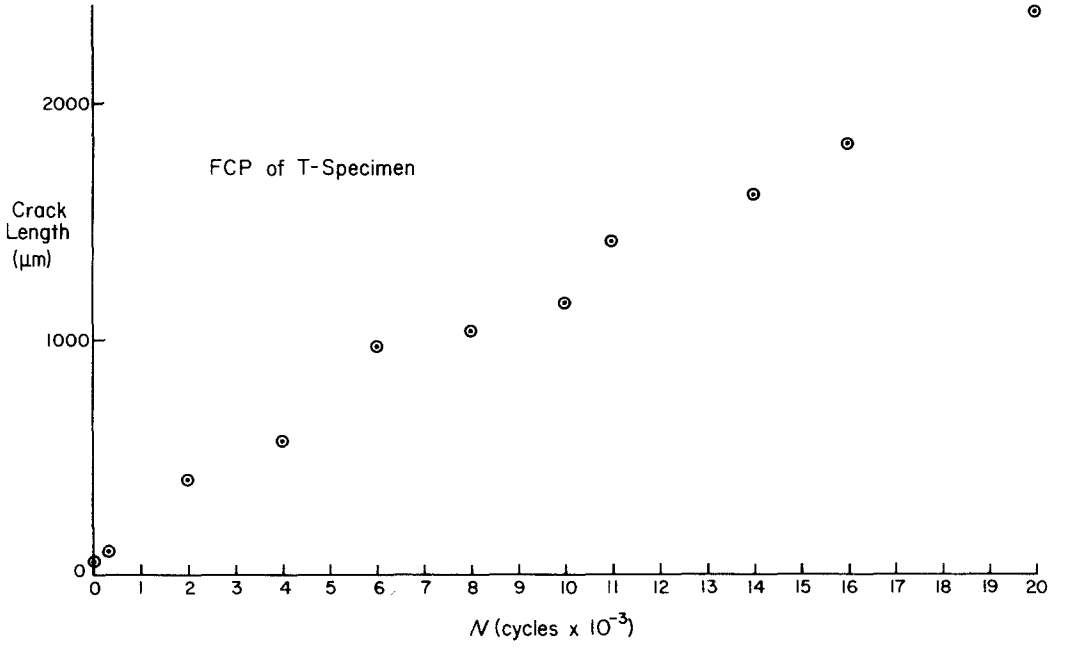

Figure 14 Fatigue crack propagation of L-specimen.

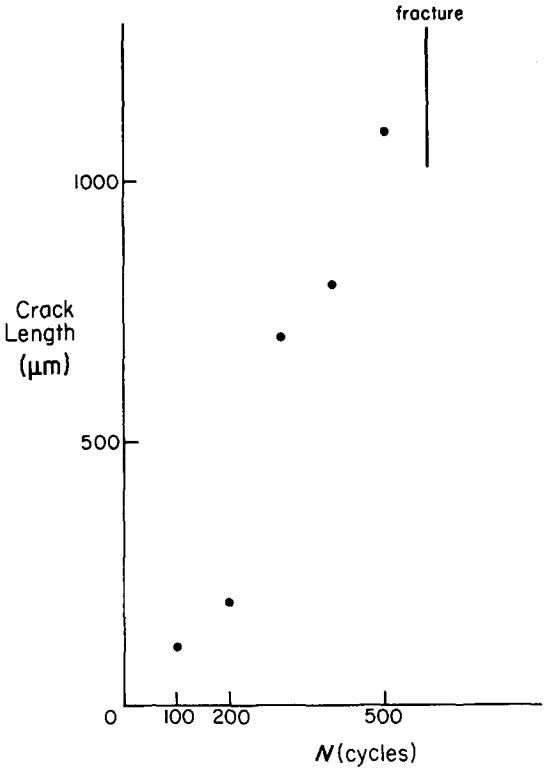

Figure 15 Fatigue crack propagation of T-specimen ($R = 0.22$, 9 kg maximum).

Such a K_c is of a macroscopic nature, based on a homogeneous and isotropic material.

The lifetime data of single layer specimens are given in Fig. 21 for three fibre orientations. There is a wide span of data points and the slope of the data band is very weak, i.e. the lifetime is nearly independent of the stress intensity at the crack tip. Data for as-moulded, three-play laminates, shown in Fig. 22, exhibits the same type of behaviour; lifetimes at a given stress intensity factor are highly spread and there is only weak slope to the data. These results parallel the crack propagation result, in which the crack velocity was also found to be independent of the stress intensity at the crack tip.

Previously, the span of lifetime data was explained by a statistical failure model based on a modified Arrhenius equation [22] and on the linear damage theory [23]. The rate process approach to fracture theory is based on the idea that the breakage of primary (chemical) bonds is thermally activated and time dependent. It has been shown that time-dependent failure plays an important role in polymers and metals. Such a linear damage theory based on this assumption may be applicable to the case of matrix fracture. Fibre fracture is believed to be nearly instantaneous. In the present case, the insensitivity of lifetime to the crack tip stress intensity factor, K_I, is another indication that microfracture far from the crack tip is paramount and that the statistical distribution of flaws and chain ends controls the fracture life.

There may be several reasons for a wide span of lifetime data:

1. The variation of specimen thickness from sample to sample (40 mils ± 5 mils).
2. The elimination of internal moulded-in stresses during machining causes a very slight warpage of specimen, even though the specimen size is reduced to remove this effect.
3. The fibre orientation is not ideal and sometimes quite random locally.

These factors appear to produce a scatter in the K_c against t_F data.

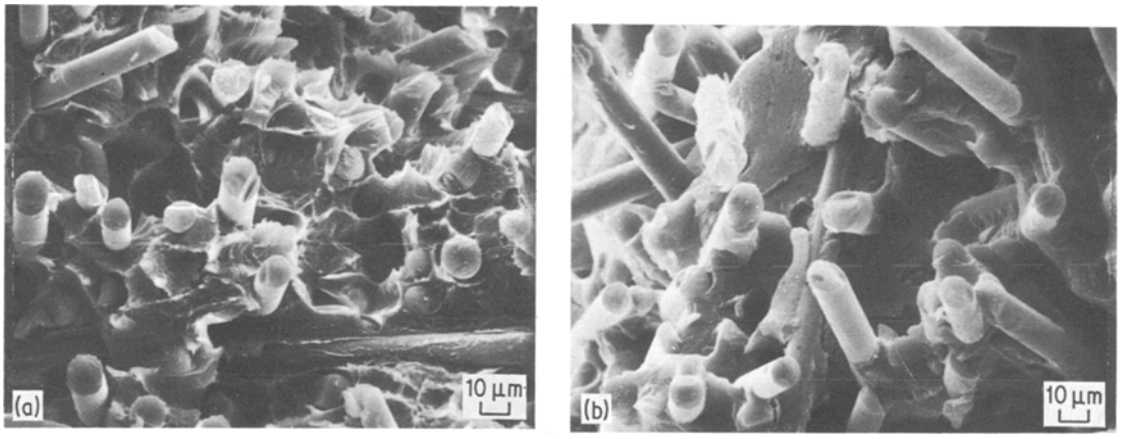

Figure 16 (a) Ductile zone (slow crack propagation) of L-specimen near notch. (b) End section: brittle matrix failure.

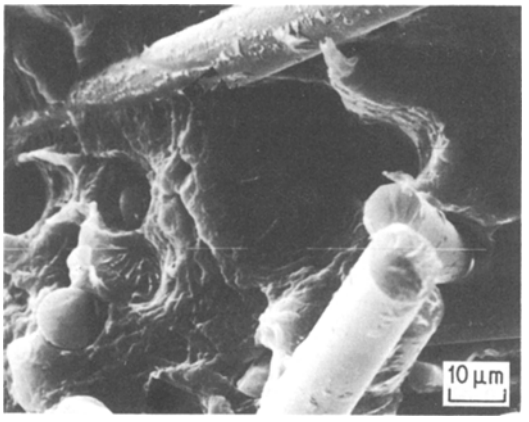

Figure 17 Magnified view of notch area of Fig. 16. Cracks start from fibre ends (arrows).

3.4. Tensile testing and K_c measurement

Tensile tests were performed on dog bone tensile bars, at a crosshead displacement rate of 0.127 cm min^{-1}. 0, 45 and 90° orientations of fibre axes with respect to the tensile axis were used. Pure resin was also tested. The composites exhibited little or no nonlinearity prior to failure. The resin itself showed an upper yield point and a large degree of plastic flow before failure.

The failure stresses σ_c of the composites are essentially the stresses σ_f of the fibre, because of the low strength and ductility of the matrix. The fibre stresses at failure are the following:

$$(\sigma_f)_L = 191.3\,\text{MPa},$$
$$(\sigma_f)_{45°} = 93.7,$$
$$(\sigma_f)_T = 68.5.$$

Using Hooke's law, the tensile moduli of the three orientations are:

$$(E)_L = 31.02\,\text{GPa},$$
$$(E)_{45°} = 13.71,$$
$$(E)_T = 13.69.$$

K_c data for constant strain-rate loading are obtained from the maxima in load–displacement curves of notched compact tension specimens. Results of such tests yield the following results:

$$(K_c)_L^{exper} = 14.5\,\text{MPa}\,\text{m}^{1/2},$$
$$(K_c)_{45°}^{exper} = 9.9\,\text{MPa}\,\text{m}^{1/2},$$
$$(K_c)_T^{exper} = 7.7\,\text{MPa}\,\text{m}^{1/2}.$$

The $(K_c)_L^{exper}$ will later be compared to a value predicted on a microscopic model. For reference, the strain at composite failure is determined to be:

$$(\epsilon)_L = 0.0061,$$
$$(\epsilon)_{45°} = 0.0068,$$
$$(\epsilon)_T = 0.005.$$

4. Discussion

4.1. Fractographic model

A short-fibre composite has many crack initiators, located chiefly at each fibre end. During the period of stress application, the stress concentration at each fibre end, as well as at the notch tip, causes fine microcracks to develop throughout the large volume of the composite. This effect is stronger near the main crack tip than in the remote areas.

When the main crack reaches a fibre, it can either pass through (fibre fracture) or go around (interface fracture). In reality, it follows the fibre/matrix interface, unless there happens to be a fibre

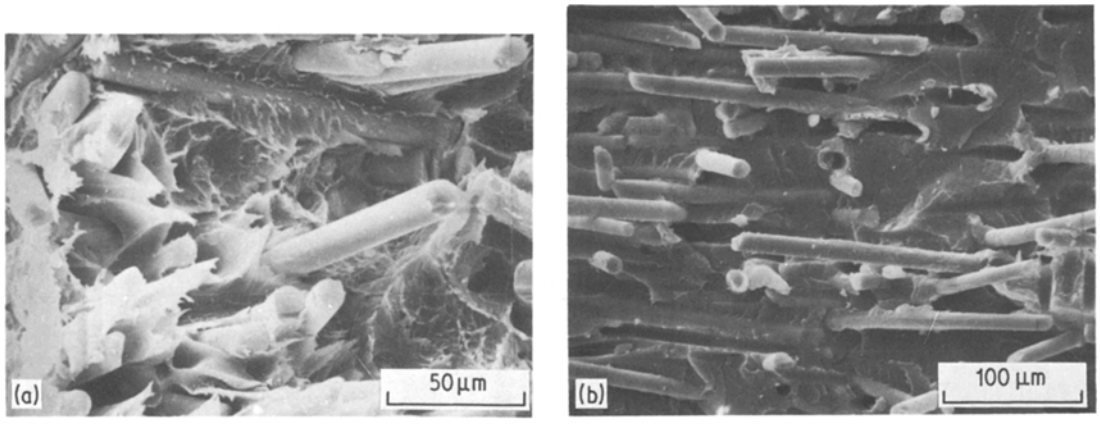

Figure 18 (a) Notch area of stress-rupture L-sample (magnified). (b) Brittle zone.

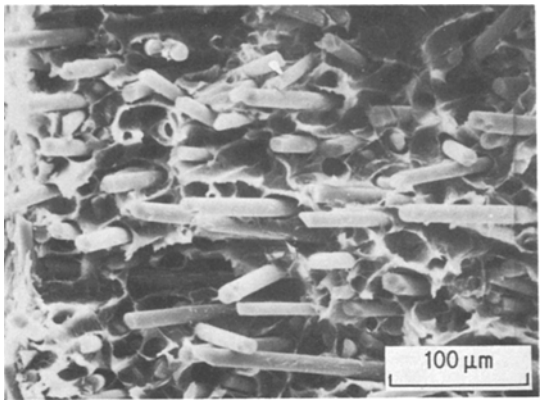

Figure 19 Quasi-impact (constant strain rate) L-specimen.

fracture induced by a neighbouring fibre end long before the main crack tip arrives.

Since the previous interface fracture is not usually complete, the crack grows along the interface until it meets the fibre tip, where it jumps to the end of another previously-developed crack (matrix fracture). But the matrix phase is relatively soft. Therefore under high load, the matrix crack grows quite rapidly to the next barrier (fibre) and repeats the process of interface fracture.

There are three incidents happening quite far from the main crack tip:

1. Fibre breakage induced locally by the combined action of normal and shear stresses.
2. Matrix cracking by local deformation from fibre ends or broken fibre sections.
3. Partial debonding of the matrix/fibre interface.

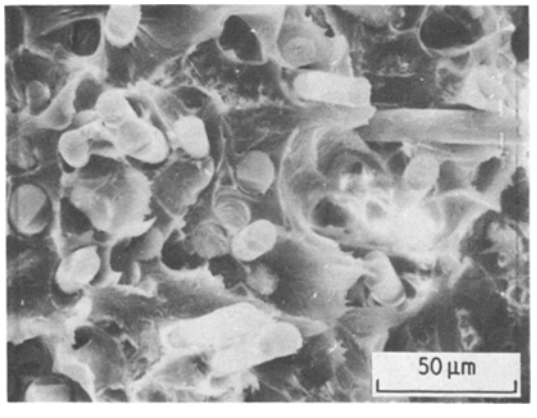

Figure 20 High-cycle fatigue fracture surface, taken from the zone of transition between brittle and ductile behaviour.

All three phenomena can contribute to the propagation of the main crack tip by ultimately connecting to the main crack through weak paths. These three modes are observed to occur far in advance of the main crack; they are induced largely by the general stress and are not significantly affected by the stress concentration near the crack tip. Such dispersed microdamage phenomena may, therefore, be termed far-field. Not all microdamage ultimately becomes connected to the main crack; in some cases there may be local connections between microflaws, with those "branches" leading nowhere. The complexity of the microstructure exhibits itself as a branchy aspect of crack propagation and localized far-field effects.

This is a structural breakdown, characterized by the complexity of co-operative interactions. Stress is not only concentrated at the main crack tip, but also at numerous fibre ends. Structural breakdown is nothing else than a connecting-up of the pre-existing microcracks along weak paths. This connecting action is also largely a far-field effect, and is only secondarily affected by the immediate field near the main crack tip. The models of far-field effects for L- and T-specimens are illustrated in Figs. 23 and 24, respectively.

The mode of final mechanical breakdown is an instantaneous catastrophe in the case of the L-configuration. Initially, the crack grows discontinuously, making numerous branches that are locally separate from each other. The locality of stress singularities induces a competition from various microcracks to join the main crack tip. A weakest path, determined by flaws and co-operative interactions, develops mainly along the interface and matrix. The applied stress is distributed among various crack branches, weakening a stress concentration on the main crack tip. As the crack grows by far-field effects, the stress concentration at the main crack tip reaches a value sufficient to cause an instantaneous fibre pull-out, fibre fracture and matrix breakage. Prior to breakdown, a crack acceleration is not found (on a very short time duration), since the increase of local stress at the crack is not of large importance.

In the case of a T-specimen, the mode of breakdown is matrix-dominated and crack acceleration can evolve. Partial debonding is accomplished by a far-field effect, before the main crack arrives, and therefore the connection of microcracks is done mainly through the matrix phase, secondarily by debonding.

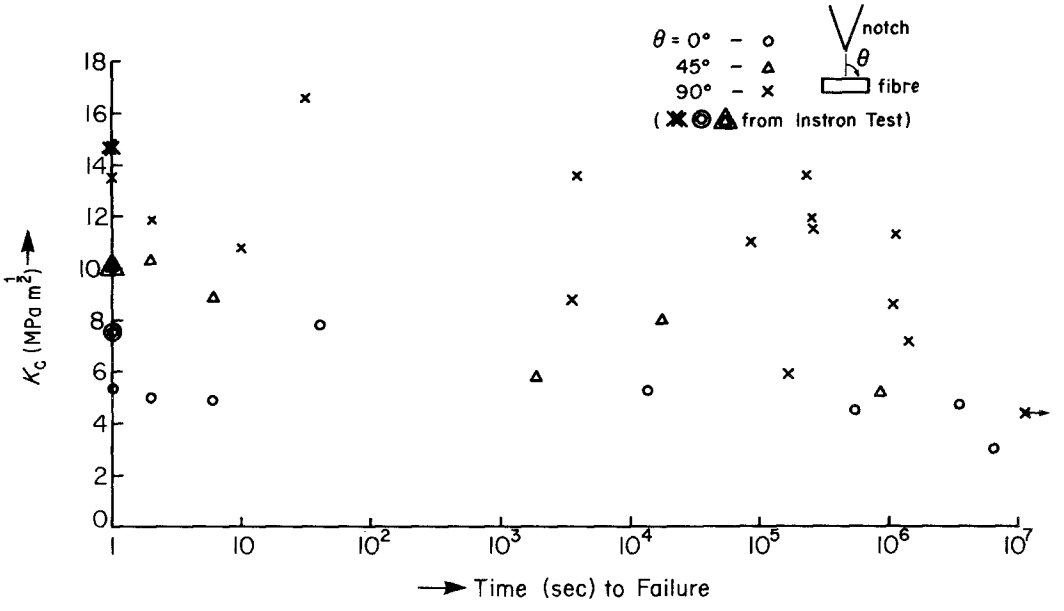

Figure 21 Initial stress intensity–time to failure data of transverse ($x \equiv 90°$), longitudinal ($o \equiv 0°$), and oblique ($\Delta \equiv 45°$) specimens of single layer.

So, the emerging fractographic model proposed in Fig. 25 has the following characteristics:

1. Weakening of the role of the stress concentration at the main crack tip.
2. Unpredictability of crack acceleration to final breakdown.
3. Discontinuous (step-wise) mode of crack growth through the far-field effect.
4. Apparent crack arrest at a local barrier.
5. The time duration of the crack acceleration stage is extremely short, sometimes instantaneous.
6. The process of time dependence comes from the interfacial debonding and apparent crack arrest.
7. Cracks are propagating in both forward and backward directions.
8. Cracks are connected through a weak path

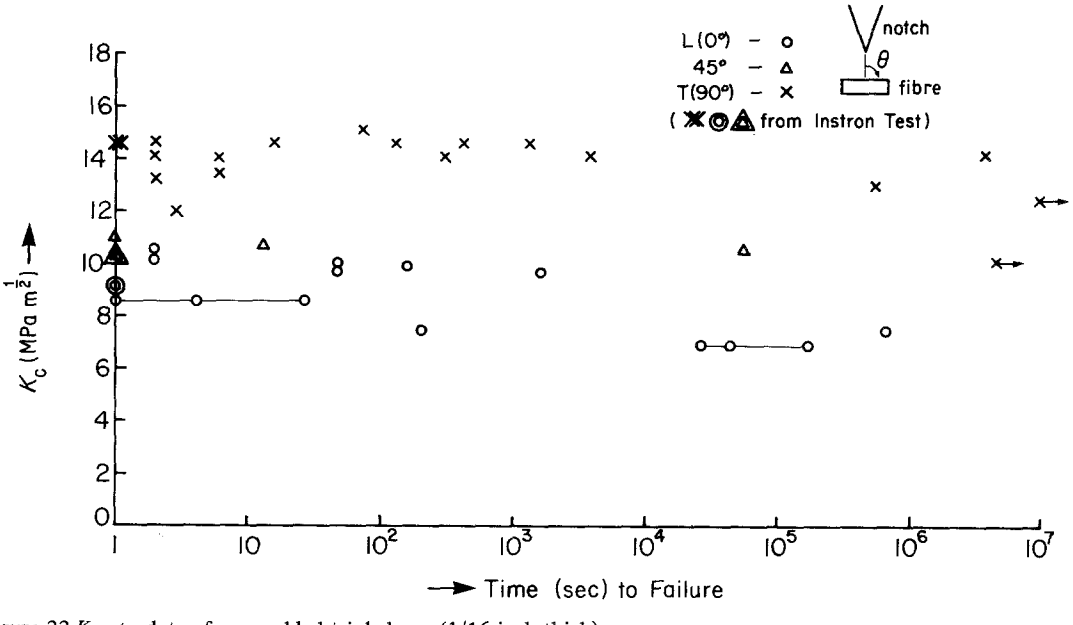

Figure 22 K_c–t_F data of as-moulded triple layer (1/16 inch thick).

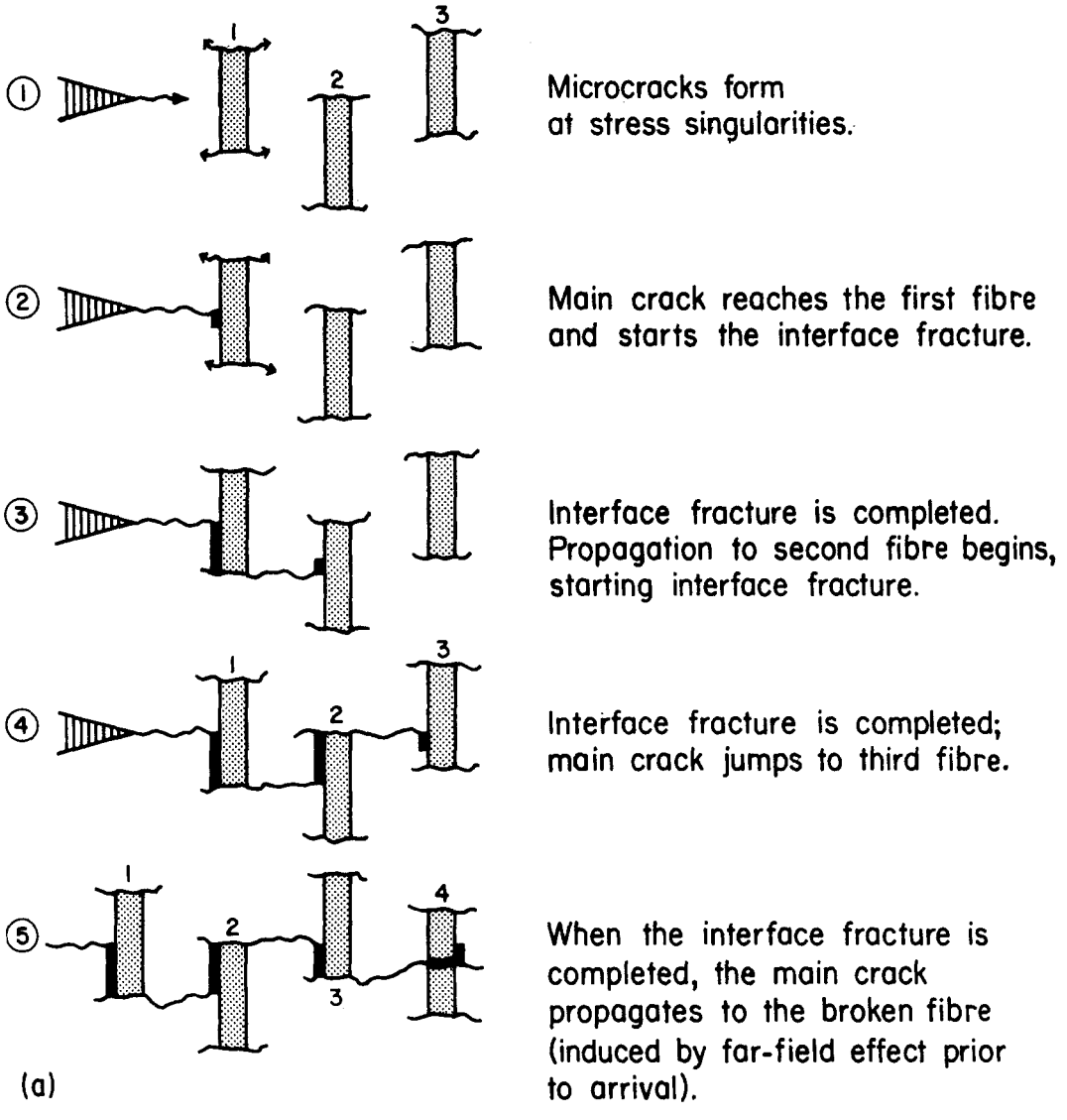

Figure 23 (a) Far-field effect of L-specimen. (b) Critical damage induced by far-field effect.

and the far-field zone is advanced. The far-field effect builds up again up to the saturation point where it jumps to the next zone.

4.2. Microscopic/macroscopic correlation

For constant strain-rate testing of L-oriented specimens (fibres parallel to testing axis), it is possible to compute the magnitudes of the several contributions – fibre fracture, fibre debonding, fibre pull-out and matrix fracture – to the work of fracture, W. The sum of these contributions can be compared to the observed total work of fracture, obtained from the stress intensity factor at failure, K_c, and the measured tensile modulus.

Microscopic modelling yields the following for the several contributions to the work of fracture:

1. Fibre fracture energy, W_f [24]

$$W_f = \frac{\pi d^2 \sigma_f^2 l_p}{6E_f} N_f. \quad (2)$$

2. Fibre debonding energy, W_d [25]

$$W_d = \frac{\pi d^2 \sigma_f^2 l_p}{4E_f} N_p. \quad (3)$$

3. Fibre pull-out energy, W_p [26]

$$W_p = \frac{\pi d^2 \sigma_f^2 l_p}{24} N_p. \quad (4)$$

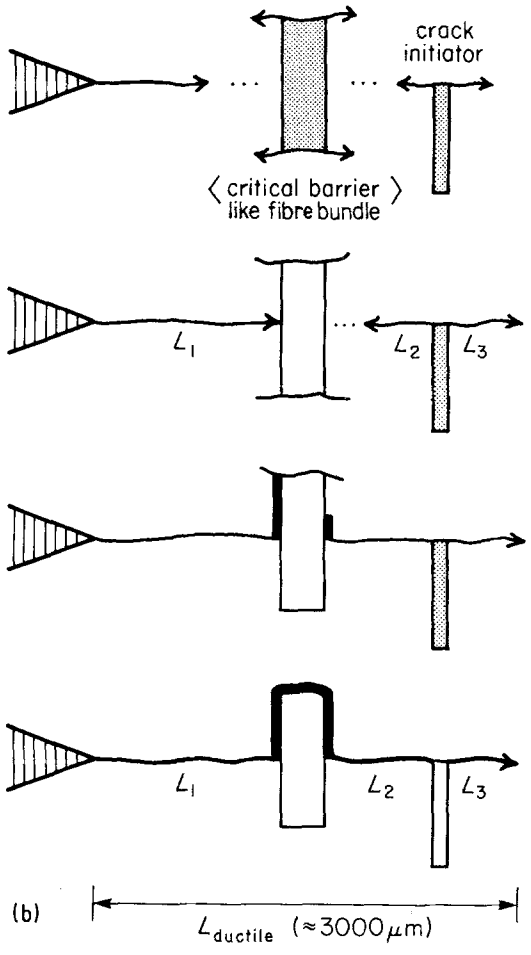

Figure 23 Continued.

4. Matrix fracture energy, W_m [27]

$$W_m = \sigma_m \epsilon_m d[(1 - v_f)^2/v_f] \quad (5)$$

For the above equations, Table I lists the definitions of the parameters, their magnitudes and the source of the magnitude evaluation. The energy contributions computed from Equations 2 to 5 are:

$$W_f = 0.4 \times 10^{-3} \text{ kg mm}^{-1},$$
$$W_d = 1.3 \times 10^{-3} \text{ kg mm}^{-1},$$
$$W_p = 478 \times 10^{-3} \text{ kg mm}^{-1},$$
$$W_m = 0.6 \times 10^{-3} \text{ kg mm}^{-1}.$$

The overwhelmingly dominant process is fibre pull-out.

The relationship between the critical stress intensity factor K_c and the total work of fracture W is

$$K_c^2 = WE = (W_f + W_d + W_p + W_m)E \quad (6)$$

where E is the composite modulus. The value of E obtained in tensile tests was 31 GPa. Inserting values for the work and modulus terms in Equation 6, the value of 11.9 MPa $m^{1/2}$ is obtained. This is in reasonable agreement with the value of 14.5 MPa $m^{1/2}$ found by tensile testing of compact tensile specimens. This agreement lends confidence to the acceptance of the individual magnitudes of W_f, W_d, W_p and W_m.

The dominance of the fibre pull-out mechanism found in relatively rapid constant strain-rate testing will not necessarily extrapolate to loading modes in which either (a) the matrix is given time to flow to eliminate local stress concentrations or (b) the fibres are put into compression over some unsupported length. In the former case, matrix crazing and rupture can supercede fibre pull-out. This change of mode is observed in dead-weight loading. In the latter case, buckled fibres can fracture in the unsupported length. This is likely the case in fatigue loading. There a fibre may partially pull out in the tensile stroke and may buckle in the compression stroke. The massive fibre fracture

TABLE I Parameters in work of fracture equations

Parameter	Definition	Magnitude	Source
d	Fibre diameter	12 μm	Direct microscopic measurement
σ_f	Composite stress at fibre failure	191.3 MPa	Tensile test
l_p	Maximum pulled-out length of fibre	500 μm	Direct microscopic measurement (Fig. 26)
E_f	Fibre modulus	72.4 GPa	[29]
N_f	Number of fibres fractured per unit area	306 mm^{-2}	Direct microscopic measurement
σ_d	Debonding stress; $\sigma_d \cong \sigma_f$	191.3 MPa	Tensile test
l_d	Average debonded length; same as average pull-out length	200 μm	Direct microscopic measurement
N_p	Number of fibres pulled out per unit area	2614 mm^{-2}	Direct microscopic measurement
σ_m	Matrix stress at failure	62.5 MPa	[28]
ϵ_m	Matrix strain at failure	0.0061	Tensile test
v_f	Volume fraction fibres	0.33	From calculation

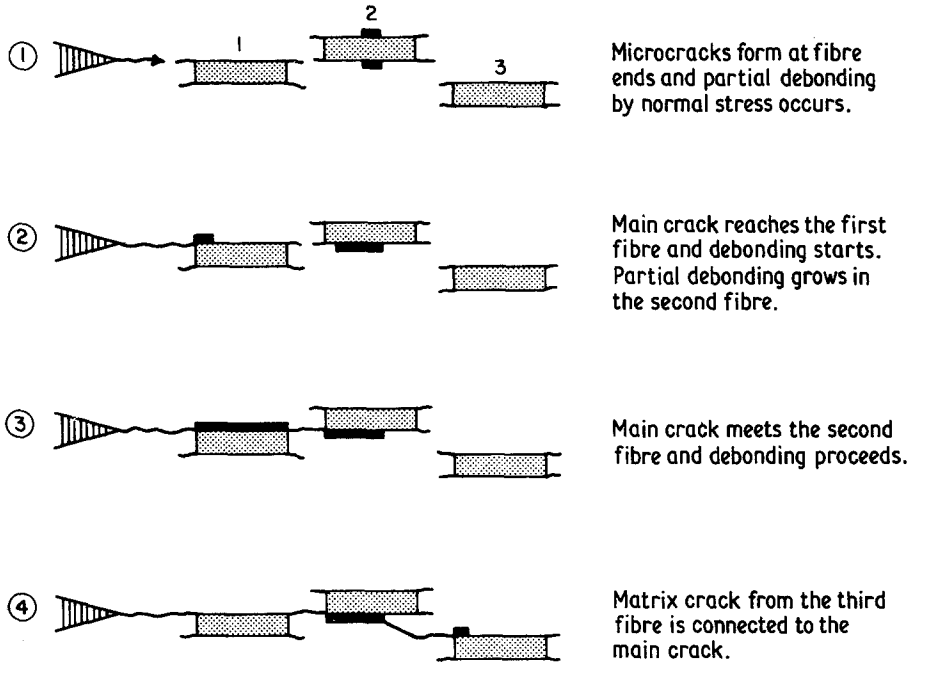

Figure 24 Far-field effect of a T-specimen.

observed in high-cycle fatigue fracture surfaces is evidence for this mechanism.

5. Conclusions

The microscopy and fracture mechanics approach to thermoplastic (PET) reinforced with E-glass short fibre revealed the following points:

1. In dead-loading and constant strain-rate loading, the crack propagates along the fibre/matrix interface and the matrix phase, the critical step being the interfacial fracture.
2. There is a sudden breakdown accomplished by the topological connection through a weak path. The part-through breakdown occurs when the modification of the effective notch geometry by the damage zone is such that sequential failure is self-catalysed; i.e. the stress gradient ahead of the incipient crack must be such that crack propagation can be self-sustaining.
3. The fibre fracture and microcracks from fibre ends are induced by a far-field effect, not by an immediate field near the crack tip.
4. There is a ductile-to-brittle transition of the matrix phase in stress-ruptured specimens from the notch to the other end. The velocity of crack propagation is related to this transitional behaviour; i.e. the slow crack propagation correlates to a ductile mode and fast propagation correlates to a brittle mode.
5. In fatigue experiments, the transitional behaviour is from brittle to ductile mode. The brittle fracture behaviour is likely due to buckling fracture of partially pulled-out fibres.

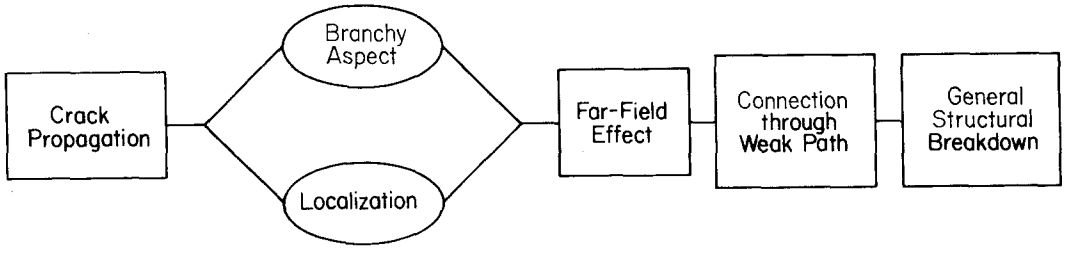

Figure 25 Fractographic model of failure.

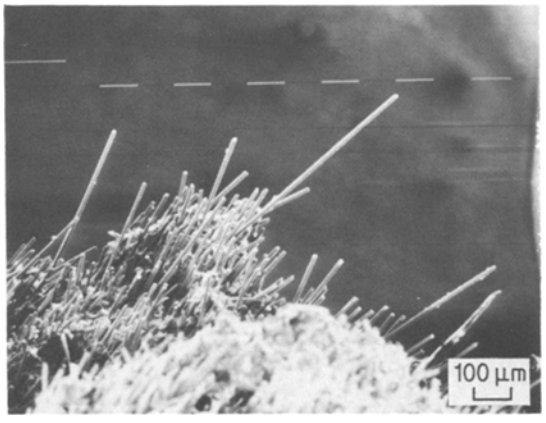

Figure 26 Distribution of fibre pull-out length for L-specimen.

6. Impact (or quasi-impact) causes a massive fibre pull-out, while fatigue causes a massive fibre fracture. Both are present in stress-rupture tests.
7. There are two bounds (lower and upper) on stress-rupture lifetime and in between these two bounds the load against lifetime data has a wide span with a very weak slope.
8. The lifetime of the L-configuration is higher than both T- and 45°-configurations. This is due to the additional fibre pull-out energy for fracture in the case of L-specimens. The fracture of T- and 45°-specimens occur mainly by matrix cracking plus partial interface debonding.
9. Fibre fracture away from the crack tip zone is aided by the shear stress induced by a neighbouring fibre end.
10. The dominant process in the work of fracture for constant strain-rate loading is fibre pull-out. It appears that this dominance does not extend to stress rupture or to high-cycle fatigue loading.

Acknowledgements

The authors are particularly grateful to Drs E. Deyrup and B. Epstein of the E. I. du Pont de Nemours and Company for supplying injection moulded Rynite® plaques, for useful consultation, and for their general support of this work.

We acknowledge, with gratitude, also the work and patience of the office and artistic staff of the Center for Composite Materials. We are indebted also to Professor R. B. Pipes, for his enthusiastic support of this programme.

References

1. K. FRIEDRICH, "Microstructure and Fracture of Fiber Reinforced Thermoplastic Polyethylene Terephthalate (Rynite®)", Report CCM-80-17, Center for Composite Materials, University of Delaware (1980).
2. *Idem, Prakt. Metallogr.* (1980).
3. *Idem, Kunststoffe* (1981).
4. JEAN C. MALZAHN, MChE thesis, University of Delaware (1982).
5. J. O. OUTWATER and M. C. MURPHY, 24th Annual Technical Conference of the Society of Plastics Industry, Washington, DC, February 1969 (SPI, Inc., New York, 1969) p. 1.
6. G. A. COOPER and A. KELLY, *J. Mech. Phys. Sol.* **15** (1967) 279.
7. C. ZWEBEN, *ibid.* **19** (1971) 103.
8. E. M. WU, Comp. Mat. Workshop, Technomic Publishing Co., Inc. (1968) 20.
9. H. J. KONISH *et al.*, *J. Comp. Mater.* **6** (1972) 114.
10. M. J. OWEN and P. T. BISHOP, *ibid.* **7** (1973) 146.
11. C. D. ELLIS and B. H. HARRIS, *ibid.* **7** (1973) 76.
12. P. W. BEAUMONT and D. C. PHILLIPS, *J. Mater. Sci.* **7** (1972) 682.
13. J. F. MANDELL, F. J. McGARRY, R. KASHIHARA and W. R. BISHOP, "Engineering Aspects of Fracture Toughness: Fiber Reinforced Laminates", 29th Annual Technical Conference of the Society of Plastics Industry 17-D, Washington, DC, February 1974 (SPI, Inc., New York, 1974) p. 1.
14. S. GAGGAR and L. J. BROUTMAN, ASTM STP 631 (American Soceity for Testing and Materials, Philadelphia, 1977) p. 310.
15. P. T. CURTIS, M. G. BADER and T. F. BAILEY, *J. Mater. Sci.* **13** (1978) 377.
16. M. G. BADER, T. W. CHOU and J. QUIGLEY, "New Developments and Applications in Composites", edited by D. Wildsdorf (The Metallurgical Society, AIME, New York, 1979).
17. H. FUKUDA and T. W. CHOU, *J. Mater. Sci.* **16** (1981) 1088.
18. C. LHYMN, MS thesis, University of Delaware (1982).
19. E. BAER, "Polymeric Materials" (ASM, Metals Park, Ohio, 1975).
20. A. T. DIBENEDETTO and G. SALEE, *Polym. Eng. Sci.* **19** (1979) 345.
21. S. T. ROLFE, "Fracture and Fatigue Control in Structures" (Prentice Hall, Inc., Englewood Cliffs, New Jersey, 1977).
22. C. C. CHINO, R. J. SHERRY and N. W. HETHERINGTON, *J. Comp. Mater.* **11** (1977) 79.
23. J. M. SCHULTZ, Treatise on Materials Science and Technology. Vol. 10. Properties of Solid Polymeric Materials, edited by J. M. Schultz (Academic Press, New York, 1977) p. 599.
24. J. FITZRANDOLPH, D. C. PHILLIPS, P. W. R. BEAUMONT and A. S. TETELMAN, *J. Mater. Sci.* **7** (1972) 289.
25. D. H. KAELBLE, *J. Adhesion* **5** (1973) 245.
26. J. K. WELLS and P. W. R. BEAUMONT, *J. Mater. Sci.* **17** (1982) 397.

27. G. A. COOPER and A. KELLY, *J. Mech. Phys. Solids* **15** (1967) 279.
28. K. M. GUPTE, PhD dissertation, University of Delaware (1981).
29. G. LUBIN, "Handbook of Composites" (Van Nostrand Reinhold Company, New York, 1982).

Received 23 August
and accepted 29 November 1982